Environmental Earth Sciences (2022) 81:194
https://doi.org/10.1007/s12665-022-10320-0

ORIGINAL ARTICLE

Modelling a basalt reactor for direct air CO_2 capture

Michael O. Schwartz[1]

Received: 21 September 2021 / Accepted: 6 March 2022 / Published online: 19 March 2022

Abstract
Ground basalt has been used as mineral fertilizer since the early thirties. Ground basalt captures CO_2 from the atmosphere and the soil pore space, raises the soil pH and reduces ocean acidification. One tonne of basalt captures 0.153–0.165 tonne CO_2, depending on infiltration rate (400–1200 mm/a), reactive surface area (3.7–15 m^2/g) and CO_2 partial pressure (41.1–3000 Pa). When the infiltration rate is high (1200 mm/a), the CO_2 capture capacity of basalt is exhausted after 9.5–11.4 years. When the infiltration rate is low (400 mm/a), the capture capacity is exhausted after 28.2–33.1 years. With the exhaustion of the capture capacity, the newly formed carbonates that sequestered CO_2 start dissolving. The dissolution is complete after 34.9–101.7 years, depending on infiltration rate, reactive surface area and CO_2 partial pressure. The reaction products are transported to the ocean via surface waters. The degree to which the fugacity of CO_2 controlled by the Henry constant exceeds the fugacity of atmospheric CO_2 along the travel path depends on many unknowns. Thus, it is impossible to reliably predict to which degree the captured CO_2 is recycled to the atmosphere, if it is recycled at all.

Keywords Climate change · Carbon dioxide · CO_2 · Basalt fertilizer · Ocean acidification · Numerical model

Introduction

Ground basalt added to agricultural fertilizer captures atmospheric carbon dioxide (CO_2), raises the soil pH, reduces ocean acidification and supplies important nutrients such as magnesium, potassium, calcium, iron and phosphorus. Ground silicate rock has been used as mineral fertilizer since the early thirties (Hilf 1938; de Villiers 1961; Gillman et al. 2002; van Straaten 2006; Anda et al. 2009). More recently, CO_2 sequestration by silicate rock has been investigated by incubation and infiltration experiments, which had reaction periods in the range of 3–12 months (ten Berge et al. 2012; Dietzen et al. 2018; Kelland et al. 2020; Amann et al. 2020). These experiments exploited only a minute fraction of the CO_2 sequestration potential. However, reactive-transport modelling with the TOUGHGHREACT software is capable of covering the full lifetime of a basalt reactor. The design of models with various environmental parameters is the subject of this paper.

The weathering of silicate rock involves the reaction with dissolved carbon species, the activities of which are controlled by the thermodynamic equilibrium between CO_2 gas in the atmosphere and soil, on one hand, and liquid CO_2, on the other hand. This is a natural process, which controls the CO_2 level of the atmosphere on the geological time scale. The only way to enhance this natural process is to increase the reactive surface area of the silicate rock by grinding.

In terms of CO_2 sequestration potential, basalt is unique. Basalt is both a highly reactive and wide-spread silicate rock. Basaltic volcanic and subvolcanic rock occupies 5.6×10^6 km^2 or 3.5% of the land surface of the Earth (Fig. 1; Hartmann and Moosdorf 2012). Important occurrences are located in South Africa, Russia, Brazil, Ethiopia, India, the USA, Iceland, Australia, and some neighbouring countries.

The capture of CO_2 from the atmosphere via chemical reaction with ground basalt rock added to agricultural fertiliser implies additional costs. These are investment costs rather than operational costs because of the long lifetime of a basalt reactor. Basalt amendment typically would constitute less than one third of the price of high-yielding agricultural land under favourable transport conditions (transport by lorry, train and/or ship). Combining the benefits of high yield induced by basalt amendment and income from CO_2 emission certificates may lead to an economically viable situation.

✉ Michael O. Schwartz
mathgeol@yahoo.de

[1] MathGeol, Postfach 101204, 30833 Langenhagen, Germany

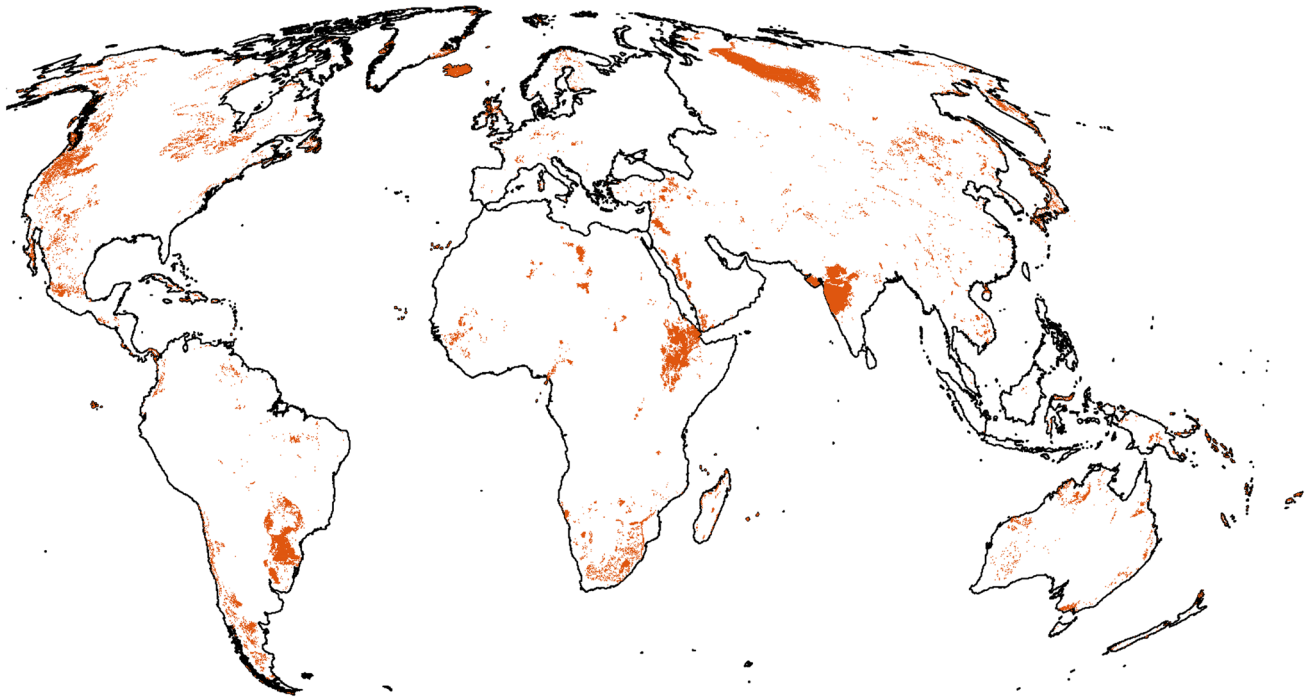

Fig. 1 Occurrences of basaltic volcanic and subvolcanic rock (Hartmann and Moodorf 2012). Equal-area Mollweide projection

Basalt amendment shares the high environmental costs of climate neutrality with other techniques such as storage of electrical energy or hydrogen production. These environmental costs arise from the mining of immense amount of rock and minerals needed for the setup-up of the emission-reducing installations.

The purpose of this research is to predict the performance of the basalt reactor as a function of reactive surface area, CO_2 partial pressure and rainwater infiltration. The research is meant to guide decision-makers in a more reliable way than previous studies with a more general approach (Taylor et al. 2015; Taylor et al. 2017; Strefler et al. 2018; Lefebvre et al. 2019; Beerling et al. 2020a).

Materials and methods

TOUGHREACT computer code

All models have been calculated with TOUGHREACT version 3. This a numerical simulation programme for chemically reactive flows of multi-phase fluids in porous and fractured media (Xu et al. 2014a). Interactions between mineral assemblages and fluids can occur under local equilibrium or via kinetic rates. The reaction rate is a function of the mineral saturation ratio and is calculated with the rate expression of Lasaga et al. (1994). This is a chemical inhibition term, which slows the dissolution/precipitation rate as the chemical state of the fluid approaches chemical equilibrium with respect to the dissolving/precipitating mineral phase.

Flow model

Base case

A structured orthogonal model mesh with three elements and horizontal dimensions of 1×1 m is used (Table 1). The top and bottom elements have a volume of 10^{52} m^3. Thus, Dirichlet conditions are imposed, i.e., the thermodynamic conditions of the top and bottom element do not change at all. The intermediate element has a volume that represents

Table 1 Flow model setup

Simulation period (a)	101.7
Model length/width (m)	1/1
Temperature (°C)	25
Total pressure (Pa)	0.999947×10^5–1×10^5
CO_2 partial pressure (Pa)	41.1–3000
Porosity (−)	0.3
Permeability (m^2)	10^{-13}
Basalt grain density (kg/m^3)	2800
Basalt reactive surface area (m^2/g)	3.7–15
Basalt application rate (t/ha)	100
Infiltration rate (mm/a)	400–1200

100 tonnes of ground basalt distributed over an area of 1 hectare (0.005 m^3). The total pressure at the top element is 10^5 Pa, and the partial pressure of CO_2 gas is set at 41.1 Pa, which is actual atmospheric partial pressure at standard conditions (10^5 Pa, 25° C). The bottom element has a total pressure of 0.999982×10^5, 0.999965×10^5 or 0.999947×10^5 Pa, which serves to maintain an infiltration rate of 400, 800 or 1200 mm/a, respectively. These infiltration rates characterize mid-latitude, subtropical and tropical climate conditions.

The rock grain density has the typical value of Columbia River basalt, US.A. (2.8 g/cm^3; DOE 1982). The remaining material parameters are taken from a CO_2 sequestration test case of Xu et al. (2014b).

Sensitivity cases

The sensitivity cases have the same setup as that of the base case but use soil CO_2 partial pressure instead of atmospheric CO_2 partial pressure. The lower limit (3×10^2 Pa) and upper limit (3×10^3 Pa) of the range given by Bohn et al. (2001) are applied.

Reactive transport model

Base case

The transport conditions are simulated for ground rock with a reactive surface area of 7.4 m^2/g determined for a grind size $P_{80}=1250$ µm (80% sieve passing size) for crushed basalt using the N_2 adsorption method (Kelland et al. 2020) and calculated with the BET equation named after Brunauer, Emmett, and Teller who developed the theory. The initial and boundary water composition is that of rainwater collected in the tropical Pune area, India (Momin et al. 2005), supplemented with Fe and Si analyses of rainwater collected in the Panipat area, India (Bharti et al. 2017), and an Al analysis of rainwater collected in the Bandung area, Indonesia (Hasan et al. 2017) (Table 2). The temperature is 25 °C. The initial and boundary partial pressure of CO_2 gas is set at 41.1 Pa, which is actual atmospheric partial pressure at standard conditions (10^5 Pa, 25 °C). This setup defines a total aqueous carbon concentration of 1.3×10^{-5} mol C per kg H_2O (molal).

The glass fraction of the basalt is 0.25, which is a typical value for Columbia River basalt, USA, such as that used by Kelland et al. (2020). The proportion of the crystallised phases corresponds to the mineralogical composition of the basalt used by Pollyea and Rimstidt (2017) (Table 3). A volume fraction of 0.02, consisting of TiO_2 and P_2O_5 components, is neglected, i.e., assumed to be non-reactive. A simplified set of reaction products is used (Pollyea and Rimstidt 2017): calcite, siderite, magnesite (i.e. carbonates representative of ankerite-dolomite solid solution; Reeder and Dollase 1989), amorphous SiO_2, Ca-montmorillonite, Na-montmorillonite and illite (i.e. Al-silicates representative of mixed-layer minerals solid solution; Meunier and Velde 1989). There are no kinetic data for solid solutions; therefore, the available data for minerals with a fixed composition must be used. Basalt glass (Pollyea and Rimstidt 2017) can only dissolve. Siderite (Knauss et al. 2005) and the remaining components (Palandri and Kharaka 2004) dissolve and precipitate under kinetic constraints. Illite is assumed to have the same rate constants as montmorillonite. The precipitation rates equal dissolution rates. The initial volume fraction of all reaction products is zero.

Table 2 Reactive transport model setup: initial composition of the liquid phase

pH (–)	5.7
Al (mol/kgH_2O)	9.7×10^{-10}
C (mol/kgH_2O)	1.3×10^{-5}
Ca (mol/kgH_2O)	1.2×10^{-4}
Cl (mol/kgH_2O)	8.9×10^{-5}
Fe (mol/kgH_2O)	2.3×10^{-9}
K (mol/kgH_2O)	1.3×10^{-5}
Mg (mol/kgH_2O)	2.4×10^{-5}
Na (mol/kgH_2O)	4.4×10^{-5}
O_2 (mol/kgH_2O)	2.7×10^{-4}
Si (mol/kgH_2O)	1.2×10^{-7}

The calculations are performed with the THERMODDEM thermodynamic database (Blanc et al. 2007), supplemented by data for basalt glass (Pollyea and Rimstidt 2017). All aqueous species of the elements shown in Table 2 were allowed to take part in the reactions.

Sensitivity cases

The sensitivity cases have the same setup as that of the base case but use the reactive surface area of the base case multiplied and divided by 2. The corresponding values are 15 and 3.7 m^2/g, respectively.

Results

Base case

The performance of the basalt reactor is monitored by the efficiency ratio. This is the CO_2/basalt weight ratio corresponding to the fraction of basalt that can be converted into carbonate minerals. The theoretical efficiency ratio is 0.211 but this value is not achievable under realistic assumptions, because basalt can react with water without the participation of aqueous carbon species.

Figure 2 shows that the efficiency ratio varies little with infiltration (0.161–0.165) at the end of the sequestration

Table 3 Reactive transport model setup: Initial volume fractions, reactive surface areas and kinetic properties

Mineral/glass	Chemical composition	Initial volume fraction (m^3/m^3)	Reactive surface area (m^2/g)
Amorphous SiO_2	SiO_2	0.0	3.7–15
Illite	$K_{0.85}Si_{3.15}Al_{2.85}O_{10}(OH)_2$	0.0	3.7–15
Calcite	$CaCO_3$	0.0	3.7–15
Siderite	$FeCO_3$	0.0	3.7–15
Magnesite	$MgCO_3$	0.0	3.7–15
Ca-montmorillonite	$Ca_{0.17}Al_{1.68}Mg_{0.33}Si_{3.99}O_{10}(OH)_2$	0.0	3.7–15
Na-montmorillonite	$Na_{0.33}Al_{1.67}Mg_{0.33}Si_4O_{10}(OH)_2$	0.0	3.7–15
Goethite	FeO(OH)	0.0	3.7–15
Glass	$SiAl_{0.358}Fe(II)_{0.189}Mg_{0.281}Ca_{0.264}Na_{0.079}K_{0.008}O_{3.315}$	0.25	3.7–15
Pyroxene	$CaAl_2O_3$	0.27	3.7–15
Plagioclase	$Ca_{0.6}Na_{0.4}Al_{1.6}Si_{2.4}O_8$	0.33	3.7–15
Forsterite	Mg_2SiO_4	0.13	3.7–15

Mineral/glass	Dissolution rate parameters							
	Acid mechanism			Neutral mechanism		Base mechanism		
	k_{25} ($mol/m^2/s$)	E_a (KJ/mol)	$n(H^+)^a$	k_{25} ($mol/m^2/s$)	E_a (KJ/mol)	k_{25} ($mol/m^2/s$)	E_a (KJ/mole)	$n(H^+)$
Amorphous SiO_2	–	–	–	5.89×10^{-13}	74.5	–	–	–
Illite	1.95×10^{-13}	48.0	0.22	3.89×10^{-15}	48.0	3.89×10^{-15}	48.0	– 0.13
Calcite	0.501	14.4	1.00	1.55×10^{-6}	23.5	3.31×10^{-4}	35.4	1.00
Siderite	9.77×10^{-4}	20.9	0.90	1.26×10^{-9}	62.8	–	–	–
Magnesite	4.17×10^{-7}	14.4	1.00	4.57×10^{-10}	23.5	6.02×10^{-6}	62.8	1.00
Montmorillonite	1.95×10^{-13}	48.0	0.22	3.89×10^{-15}	48.0	3.89×10^{-15}	48.0	– 0.13
Goethite	–	–	–	1.15×10^{-8}	86.5	–	–	–
Glass	5.37×10^{-5}	39.7	1.01	–	–	1.00×10^{-11}	38.4	– 0.26
Pyroxene	1.50×10^{-7}	78.0	0.70	1.07×10^{-12}	78.0	–	–	–
Plagioclase	1.35×10^{-8}	42.1	0.63	1.23×10^{-11}	45.2	–	–	–
Forsterite	1.41×10^{-7}	67.2	0.47	2.29×10^{-11}	79.0	–	–	–

[a]k_{25} is the kinetic rate constant at 25 °C; E_a is the Arrhenius activation energy; $n(H^+)$ is the reaction order with respect to H +

period. But the time spam for reaching the end of the sequestration period is strongly influenced by the infiltration rate. At tropical conditions (1200 mm/a), the end point is reached after 11.2 years. At mid-latitude conditions (400 mm/a), the end point is reached after 33.1 years.

The end point is reached when all basalt glass and forsterite have dissolved (Fig. 3). Although dissolution of plagioclase and pyroxene continue beyond the end point, the activities of aqueous Ca, Mg and Fe species remain too low for stabilizing previously precipitated carbonate minerals. The net effect is the reduction of the SmCO2 value (mass of CO_2 sequestered in solid mineral phases). All previously precipitated carbonate minerals are completely dissolved after 36.5 years and 101.7 years in the 1200 mm/a and 400 mm/a scenarios, respectively.

It is implicitly assumed that CO_2 originally sequestered via solid carbonate phases is not recycled to the atmosphere but stored in the geosphere and hydrosphere. Nevertheless, field studies that support such an assumption have not been conducted yet (Kelland et al. 2020).

Sensitivity cases

Multiplying the reactive surface area of the base case (7.4 m^2/g) by 2 has hardly any positive effect on the efficiency ratio (Fig. 2). In contrast, dividing the base case value by 2 has a significant negative effect on the efficiency ratio especially when the infiltration rate is high. This implies that there is no point in finer grinding to achieve a reactive surface area > 7.4 m^2/g. However, coarser grinding resulting in a reactive surface area < 7.4 m^2/g risks to jeopardize the performance of the basalt reactor especially under tropical conditions with a high infiltration rate.

The variations of the CO_2 partial pressure have little influence on the efficiency ratio at the end of the sequestration period (Fig. 4). But the time span for reaching the end of

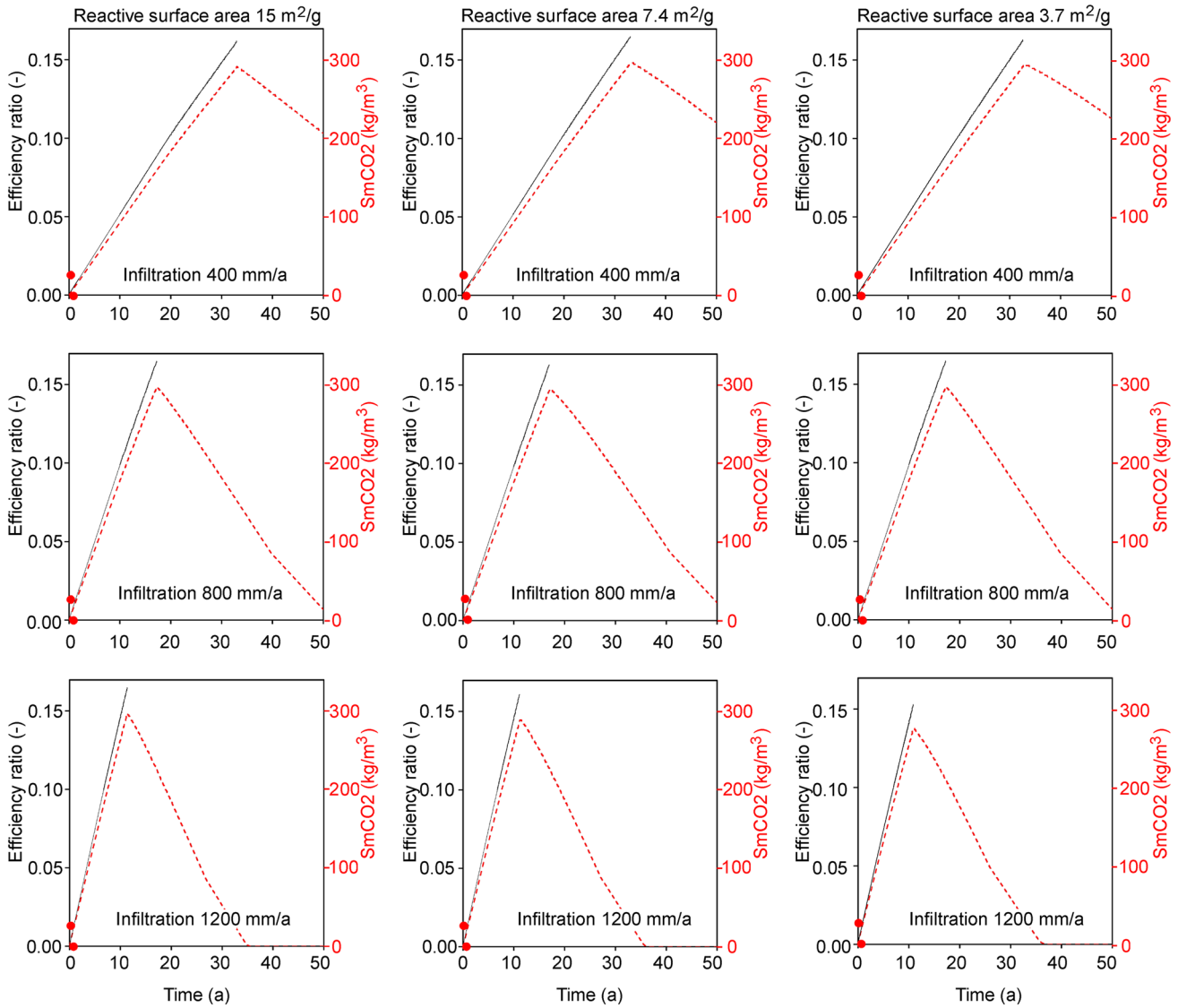

Fig. 2 Basalt reactors with 41.1 Pa CO_2 partial pressure and various combinations of infiltration rate and reactive surface area. Efficiency ratio (CO_2/basalt weight ratio; see text; black solid line; vertical scale text in black) and SmCO2 (total CO_2 sequestered in mineral phases in kg/m^3 medium; red interrupted line; vertical scale text in red) plotted versus time. Efficiency ratios obtained from infiltration experiments (red point symbols; see text) are shown for comparison

CO_2 sequestration decreases significantly when the CO_2 partial pressure is high. For example, the infiltration case with 400 mm/a has the end point at 28.2 years at 3000 Pa partial pressure; the corresponding value for a low partial pressure (41.1 Pa) is 33.1 years. The infiltration case with 1200 mm/a has the end point at 9.5 years; the corresponding value for a low partial pressure (41.1 Pa) is 11.4 years.

Comparison with experiments

The comparison of the TOUGHREACT model with experimental results is not straightforward because these are recorded in terms of release of Mg (±Ca) from dissolving ground rock but not in terms of precipitated solid carbonates. The duration, infiltration rate, type of media and ground rock loading of the experiments are

1. 0.33-year infiltration (766 mm/a) into ground basalt mixed with soil containing cereal plants, the rock loading being 100 t/ha (Kelland et al. 2020)
2. 0.61-year infiltration (213 mm/a) into forsterite-dominated olivine (the most reactive mineral component of basalt) mixed with soil containing ryegrass plants, the rock loading being 204 t/ha (ten Berge et al. 2012)
3. 1-year infiltration (800 mm/a) into ground dunite (an ultrabasic plutonic rock mainly composed of olivine)

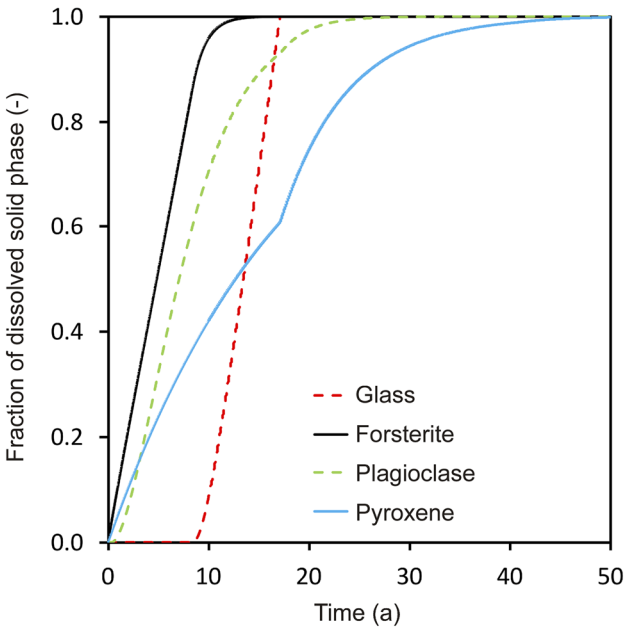

Fig. 3 Basalt reactor with a CO_2 partial pressure of 41.1 Pa, reactive surface area of 7.4 m^2 and infiltration rate of 800 mm/a. Fraction of dissolved mineral phases (forsterite, plagioclase and pyroxene) and glass plotted versus time

mixed with soil containing cereal plants, the rock loading being 220 t/ha (Amann et al. 2020).

The efficiency ratio of the experiments is higher or lower than that of the TOUGHREACT model (Figs. 2 and 4, Table 4):

1. The modelled efficiency ratio after 0.33 year infiltration is in the range of 0.0018–0.0057, i.e., lower than the experimental value (0.013)
2. The modelled efficiency ratio after 0.61 year infiltration is in the range of 0.0031–0.011, the maximum value being slightly lower than the experimental value (0.013)
3. The modelled efficiency ratio after 1 year infiltration is in the range of 0.0051–0.018, i.e., the whole range is higher than the experimental value (0.0002).

In summary, the experiments do neither confirm nor contradict the TOUGHREACT model.

Comparison with previous models

Two reactive-transport models with a simulation period that extends beyond that of the experiments with a basalt reactor have been published (1 year, Beerling et al. 2020b; 5 years, Kelland et al. 2020). Owing to the restriction of the software used (PHREEQC, Parkhurst and Appelo 2013), all precipitating phases react under equilibrium conditions. The result is a strongly non-linear relationship between efficiency ratio and time. This is in stark contrast to the near-linear relationship of the TOUGHREACT model with both dissolving and precipitating phases reacting under kinetic constraints. Preference should be given to the TOUGHREACT model, because the PHREEQC model relies on unphysical assumptions. All participating minerals precipitate under kinetic constraints with reaction rates that are at least as low as the dissolution rates (Palandri and Kharaka 2004, and references therein).

Conclusion

The modelling of the basalt reactor succeeded in predicting its efficiency ratio (0.153–0.165 tonne CO_2 per tonne ground rock) and its lifetime (9.5–33.1a) as a function of the reactive surface area, CO_2 partial pressure and infiltration rate. These results are useful for decision-makers. E.g., the combined production costs and 300 km transportation costs for ground basalt are $ 82 US per tonne for a grind size of 50 µm (Strefler et al. 2018). Accordingly, the costs for capturing one tonne of CO_2 are in the range from $ 496 US to $ 536 US. These costs are considerably less than the costs of the alternative adsorption/absorption method of direct air CO_2 capture if the obligatory CO_2 underground injection is included. For the above-ground adsorption/absorption unit alone, Viebahn et al. (2019) quote $ 540 US per tonne of captured CO_2 for both the Climeworks installation, Switzerland, and the Carbon Engineering installation, Canada, a recipient of the Gates Foundation. Including underground storage in Iceland basalt, Climeworks charges EURO 960 ($ 1100 US) per tonne CO_2 compensation in 2021 (Niemann 2021).

The permanent and safe underground storage of CO_2 is an expensive enterprise with considerable technical, geological and environmental problems. For underground CO_2 injection on the large scale, there is no easy solution in sight. To date, there is no major on-land operation for injecting CO_2 derived from an industrial source except for the petroleum industry. However, the petroleum industry is a very special case because CO_2 is obtained as an unwanted by-product during gas or petroleum exploitation and is reinjected close to its original source.

The optimal underground target for injecting CO_2 captured with a physical (non-reactive) method is basalt where CO_2 is converted into solid carbonates (Schwartz 2020);

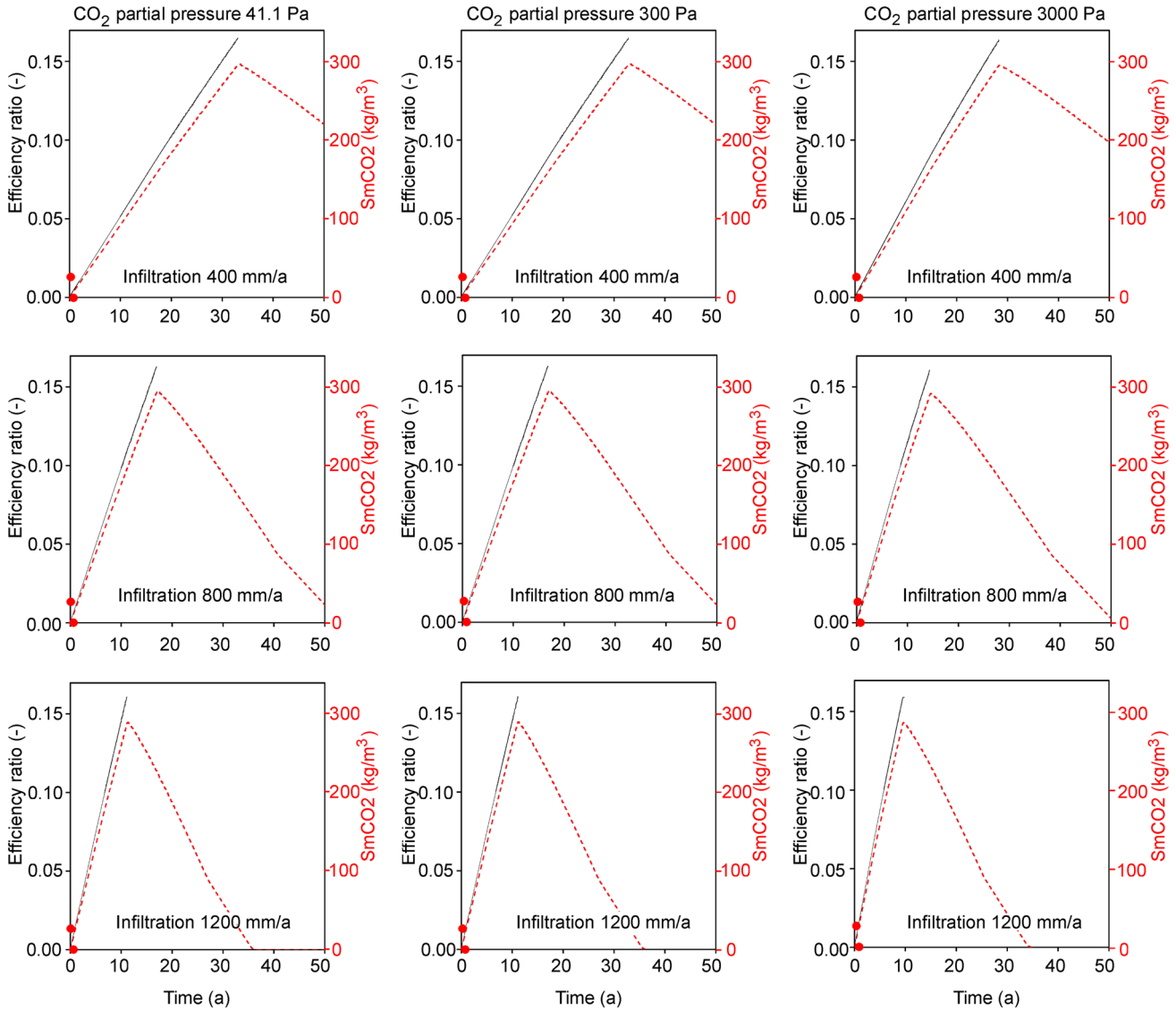

Fig. 4 Basalt reactors with a reactive surface area of 7.4 m^2 and various combinations of infiltration rate and CO_2 partial pressure. Efficiency ratio (CO_2/basalt weight ratio; see text; black solid line; vertical scale text in black) and SmCO2 (total CO_2 sequestered in mineral phases in kg/m^3 medium; red interrupted line; vertical scale text in red) plotted versus time. Efficiency ratios obtained from infiltration experiments (red point symbols; see text) are shown for comparison

whereas non-reactive target rocks such as sandstone imply the risk that injected CO_2 may leak to a near-surface aquifer and pollute the groundwater (Schwartz 2014, and references therein).

Underground CO_2 injection into basalt and mining of basalt for fertilizer production are likely to compete for space if conducted on a large scale. About 3.5% of the Earth's surface is occupied by basalt but only a minor fraction has the transport infrastructure that allows a reasonably economic use of these basalt resources. In summary, the CO_2 direct air capture is bound to encounter many obstacles. Nevertheless, modelling direct air capture is a useful comparative tool for demonstrating the advantages of reducing greenhouse gas emissions at the source.

Table 4 Comparison of experiments and models for direct air CO_2 capture

Experiment/model type	Infiltration rate (mm/a)	Ground rock material	Rock loading (t rock/ha)	Grind size	Reactive surface area (m^2/g)	Incubation/infiltration period (a)	Efficiency ratio (–)	References
Incubation	–	Olivine	50	$P_{50}=20$ µm	n.a	0.25	0.083	Dietzen et al. (2018)
Infiltration	213	Olivine	204	$P_{73}=50$ µm	4.8	0.61	0.013	ten Berge et al. (2012)
Infiltration	800	Dunite	220	$P_{50}=62$ µm	n.a	1	0.0002	Amann et al. (2020)
Infiltration	766	Basalt	100	$P_{1250}=1250$ µm	7.4	0.33	0.013	Kelland et al. (2020)
Infiltration	400	Basalt	100	–	7.4	33.1	0.165	This paper[a]
Infiltration	800	Basalt	100	–	7.4	17.1	0.164	This paper[a]
Infiltration	1200	Basalt	100	–	7.4	11.2	0.161	This paper[a]

[a]CO_2 partial pressure 41.1 Pa

Funding The authors have not disclosed any funding.

Declarations

Conflict of interest The author has no competing interests.

References

Amann T et al (2020) Enhanced weathering and related element fluxes - a cropland mesocosm approach. Biogeosciences 17:103–119

Anda M, Shamshuddin J, Fauziah CI, Omar SRS (2009) Dissolution of ground basalt and its effect on oxisol chemical properties and cocoa growth. Soil Sci 174:264–271

Beerling DJ et al (2020a) Potential for large-scale CO_2 removal via enhanced rock weathering with croplands. Nature 583:242–248

Beerling DJ et al (2020b) Potential for large-scale CO_2 removal via enhanced rock weathering with croplands. Nature. https://doi.org/10.1038/s41586-020-2448-9

Bharti PK, Singh V, Tyagi PK (2017) Assessment of rainwater quality in industrial area of rural Panipat (Haryana), India. Arch Agric Environ Sci 2:219–223

Blanc P, Lassin A, Piantone P (2007) THERMODDEM a data base devoted to waste minerals. BRGM, Orléans, France. http://thermoddem.brgm.fr

Bohn HL, McNeal BL, O'Connor GA (2001) Soil chemistry. Wiley, New York

De Villiers ODH (1961) Soil rejuvenation with crushed basalt in Mauritius. Int Sugar J 63:363–364

Dietzen C, Harrisona R, Michelsen-Correac S (2018) Effectiveness of enhanced mineral weathering as a carbon sequestration tool and alternative to agricultural lime: an incubation experiment. Int J Greenhouse Gas Control 74:251–258

DOE (1982) Site characterization report for the Basalt Waste Isolation Project. US Department of Energy (DOE) DOE/RL 82–3, Volume II

Gillman GP, Burkett DC, Coventry RJ (2002) Amending highly weathered soils with finely ground basalt rock. Appl Geochem 17:987–1001

Hartmann J, Moosdorf N (2012) A new global lithological map database GLiM: a representation of rock properties at the Earth surface. Geochem Geophys Geosyst 13(12):1–37

Hasan NY, Driejana, Sulaeman A (2017) Composition of ions and trace metals in rainwater in Bandung City, Indonesia. Proceedings Third International Conference on Civil Engineering Research (ICCER), August 1st-2nd 2017, Surabaya, Indonesia

Hilf H (1938) Die Düngung mit Basaltabfällen (The fertilization with basalt waste). Forstarchiv 14:93–101

Kelland ME et al (2020) Increased yield and CO_2 sequestration potential with the C_4 cereal Sorghum bicolor cultivated in basaltic rock dust-amended agricultural soil. Glob Change Biol 26:3658–3676

Knauss KG, Johnson JW, Steefel CI (2005) Evaluation of the impact of CO_2, co-contaminant gas, aqueous fluid and reservoir rock interactions on the geologic sequestration of CO_2. Chem Geol 217:339–350

Lasaga AC, Soler JM, Ganor J, Burch TE, Nagy KL (1994) Chemical weathering rate laws and global geochemical cycles. Geochimica Cosmochimica Acta 58:2361–2386

Lefebvre D et al (2019) Assessing the potential of soil carbonation and enhanced weathering through life cycle assessment: a case study for Sao Paulo State, Brazil. J Clean Prod 233:468–481

Meunier A, Velde B (1989) Solid solutions in I/S mixed-layer minerals and illite. Am Miner 74:1106–1112

Momin GA et al (2005) Study of chemical composition of rainwater at an urban (Pune) and a rural (Sinhagad) location in India. J Geophys Res 110(issue D8):1–24

Niemann A (2021) Saugen für das Klima. Frankfurter Allgemeine Sonntagszeitung 44:42

Palandri JL, Kharaka YK (2004) A compilation of rate parameters of water-mineral interaction kinetics for application to geochemical modeling. U.S. Geological Survey Open File Report 2004–1068

Parkhurst DL, Appelo CAJ (2013) Description of input and examples for PHREEQC version 3—a computer program for speciation, batch-reaction, one-dimensional transport, and inverse geochemical calculations: U.S. Geological Survey Techniques and Methods book 6, chap. A43

Pollyea RM, Rimstidt JD (2017) Rate equations for modeling carbon dioxide sequestration in basalt. Appl Geochem 81:53–62

Reeder RJ, Dollase WA (1989) Structural variation in the dolomite-ankerite solid-solution series: an X-ray, Mössbauer, and TEM study. Am Miner 74:1159–1167

Schwartz MO (2014) Modelling leakage and groundwater pollution in a hypothetical CO_2 sequestration project. Int J Greenhouse Gas Control 23:72–85

Schwartz MO (2020) Can CO_2 sequestration in basalt efficiently reduce greenhouse gas emission? Environ Technol. https://doi.org/10.1080/09593330.2020.1815859

Strefler J, Amann T, Bauer N, Kriegler E, Hartmann J (2018) Potential and costs of carbon dioxide removal by enhanced weathering of rocks. Environ Res Lett 13:1–26

Taylor LL et al (2015) Enhanced weathering strategies for stabilizing climate and averting ocean acidification. Nat Clim Chang 6:402–406

Taylor LL, Beerling DJ, Quegan S, Banwart SA (2017) Simulating carbon capture by enhanced weathering with croplands: an overview of key processes highlighting areas of future model development. Biol Let 13:1–8

ten Berge HM et al (2012) Olivine weathering in soil, its effects on growth and nutrient uptake in Rygrass (*Loium perenne* L.): a plot experiment. PLoS ONE 7(8):e42098. https://doi.org/10.1371/journal.pone.0042098

van Straaten P (2006) Farming with rocks and minerals: challenges and opportunities. An Acad Bras Ciênc 78:731–747

Viebahn P, Scholz A, Zelt O (2019) Entwicklungsstand und Forschungsbedarf von Direct Air Capture—Ergebnis einer multidimensionalen Analyse. Energiewirtschaftliche Tagesfragen 69:29–33

Xu T, Sonnenthal E, Spycher N, Zheng L (2014a) TOUGHREACT V3.0-OMP reference manual: a parallel simulation program for non-isothermal multiphase geochemical reactive transport. Earth Sciences Division, Lawrence Berkeley National Laboratory, Berkeley, USA

Xu T, Sonnenthal E, Spycher N, Zheng L (2014b) TOUGHREACT V3.0-OMP sample problems. Earth Sciences Division, Lawrence Berkeley National Laboratory, Berkeley, USA